Journal of Power Sources 271 (2014) 570–581

Contents lists available at ScienceDirect

Journal of Power Sources

journal homepage: www.elsevier.com/locate/jpowsour

A double-fuzzy diagnostic methodology dedicated to online fault diagnosis of proton exchange membrane fuel cell stacks

Zhixue Zheng [a, b, *], Marie-Cécile Péra [a, b], Daniel Hissel [a, b], Mohamed Becherif [a, c], Kréhi-Serge Agbli [a, b], Yongdong Li [d]

[a] FCLAB Research Federation, FR CNRS 3539, FEMTO-ST/Energy Department, UMR CNRS 6174, France
[b] University of Franche-Comté, 90010 Belfort Cedex, France
[c] University of Technology of Belfort-Montbéliard, 90010 Belfort Cedex, France
[d] Department of Electrical Engineering, Tsinghua University, 100084 Beijing, China

HIGHLIGHTS

- An automatic non-model based diagnostic methodology is developed.
- EIS measurements are used as a basic tool.
- Two features are proved to be valuable for water management issue.
- High interpretability, computational efficiency and portability can be achieved.

ARTICLE INFO

Article history:
Received 27 February 2014
Received in revised form
17 July 2014
Accepted 21 July 2014
Available online 19 August 2014

Keywords:
PEMFC
Fuzzy clustering
Fuzzy logic
EIS
Fault diagnosis

ABSTRACT

To improve the performance and lifetime of the low temperature polymer electrolyte membrane fuel cell (PEMFC) stack, water management is an important issue. This paper aims at developing an online diagnostic methodology with the capability of discriminating different degrees of flooding/drying inside the fuel cell stack. Electrochemical impedance spectroscopy (EIS) is utilized as a basis tool and a double-fuzzy method consisting of fuzzy clustering and fuzzy logic is developed to mine diagnostic rules from the experimental data automatically. Through online experimental verification, a high interpretability and computational efficiency of the proposed methodology can be achieved.

1. Introduction

Features such as high efficiency, environmental friendliness and high availability rating make fuel cell (FC) an attractive power converter for a wide variety of applications ranging from portable and transportation to large-scale stationary applications [1]. Among the existing FC technologies, polymer electrolyte membrane fuel cell (PEMFC) is considered as a lead candidate for the next generation power sources, considering its noteworthy characteristics like low operating temperature (50–100 °C), high power density, low weight and compactness, fast start-up and suitability for discontinuous operations [1–3]. Invented in the early 1960s by Thomas Grubb and Leonard Niedrach from General Electric, PEMFC has not received much attention until a couple of decades ago. During this period, remarkable breakthroughs including the introduction of the Nafion membrane, platinum-loading improvement and catalyst-ink technique for electrodes have been achieved and have promoted its further applications [3].

Nevertheless, before its full commercialization, three primary barriers need to be overcome: large supply of high-purity hydrogen, cost reduction and increased durability [1,3]. The traditional way of producing hydrogen is still by reforming oil or natural gas today, which causes inevitable greenhouse-gas emissions. Water electrolysis using electricity is thus also a research focus. Recent developments include producing hydrogen using electricity supplied by wind turbines or photovoltaic panels [1]. For the second barrier, the cost of the PEMFC system can be generally divided

* Corresponding author. FCLAB Research Federation, FR CNRS 3539, FEMTO-ST/Energy Department, UMR CNRS 6174, France.
E-mail addresses: zhixue.zheng@femto-st.fr, zhixueying@126.com (Z. Zheng).

http://dx.doi.org/10.1016/j.jpowsour.2014.07.157
0378-7753/

into two parts: FC cost and auxiliaries cost. According to the US Department of Energy (DoE) 2012 report, FC cost has been declined more than 83% since 2002 and 36% since 2008. In 2012, a cost of 47 $/kW was estimated for 80-kW net PEMFC systems given that 500,000 units/year are produced [4]. However, compared with traditional internal combustion engine systems, the cost is still more than twice even in this favorable estimation [3]. As for the durability, although remarkable progresses have been made during the recent years, compared with the DoE 2010 targets (5000 h for the transportation and 40,000 h for stationary power generation), substantial technical gaps still exist [5]. A lifetime of 2500 h for transportation PEMFC stack was reported in Ref. [3].

In the scope of this study, the last barrier, i.e., durability of the FC system, is the focus. Herein, water management inside the PEMFC stack is an important issue in order to improve its performance and lifetime. On one hand, proper membrane humidity should be maintained to guarantee good proton conductivity. On the other hand, excessive liquid water may block the pores in the catalyst layer or gas diffusion layer and lead to a difficult mass transfer process [6].

Various methods have been proposed in the literature to detect water behavior inside the FC. One category is model-based method, which involves both analytical and black-box models [7]. Hernandez et al. [8] developed an electrical equivalent circuit of a PEMFC system based on charge, matter and energy conservation laws. A global model was built taking into account of both FC stack and ancillary circuits including hydrogen, air, cooling and humidification circuits. The developed model allows the detection of flooding, drying and membrane deterioration through observing the variations of several crucial parameters in the circuit. Although a high interpretability and generality can be achieved by this kind of method, extensive assumptions, complicated parameter identifications and a high computational cost are required, which have limited its further applicability for online diagnosis [9]. In addition, a master of the system physical and operational knowledge is essential [7]. Compared with analytical models, black-box ones provide an interesting alternative especially in the case of modeling uncertainty or the presence of incomplete knowledge in the system [10]. An example of black-box model based on neural network was developed in Ref. [11]. Two individual Elman recurrent neural networks (ENN) composed of three layers were constructed with four inputs (stack current, air inlet flow rate, stack temperature and dew point temperature) and two outputs (stack voltage and the cathode pressure drop). Stack voltage was used as the diagnosis basis while the pressure drop was employed as a discriminating parameter. Despite the fewer requirements of system physical knowledge and higher computational efficiency compared with analytical method, a big inconvenience of black-box one exists in its low transparency and poor interpretability for human users.

Another category for water behavior detection is known as a non-model based method, which is also called pattern recognition method in some literature [12]. Compared with model-based one, it is quite promising for online applications due to its simplicity and computational efficiency. In Ref. [13], the dominant frequency of the pressure drop signal was utilized as a diagnostic tool of water behavior in PEMFC. In Ref. [14], wavelet transform analysis of stack voltage was used for discriminating flooding and non-flooding. However, to our best knowledge most of the non-model based methods reported in literature are limited to offline application.

In this paper, a double-fuzzy diagnostic methodology in combination with EIS measurements is proposed to monitor water behavior in the PEMFC stack online. It belongs to the category of non-model based method. The meaning of double-fuzzy consists in a fuzzy clustering method for forming data clusters and a fuzzy logic approach for decision-making based on the clustering results. To our best knowledge, this work is a first attempt to apply a combination of fuzzy logic and fuzzy clustering in the domain of FC online diagnosis. The reasons why fuzzy methods are utilized here include:

(1) The high uncertainty contained in the target problem. The terms such as “severe drying (flooding)”, “medium drying (flooding)” and “slight drying (flooding)” are more fuzzy than crisp; In addition, it is usually hard to determine the precise boundaries between different classes especially when transitory states exist.
(2) Incomplete human knowledge. Despite the increasing scientific evolution of the FC technology, their inherent complexity makes its fault diagnosis a rather difficult task. Indeed, FC systems combine knowledge in different areas, such as electrochemistry, thermodynamics, fluid dynamics, electricity, etc [8]. To establish a reasonable analytical model of the system, a high degree of knowledge in the above areas is required, which makes the task quite complicated. Fuzzy methods provide an interesting alternative in the presence of incomplete or ambiguous knowledge about a system.
(3) The requirement of high interpretability. Interpretability, i.e., easy to read and be understandable by human, is a fundamental factor determining the acceptability and the usability of a diagnostic methodology for online applications [15]. Fuzzy logic mimics human's way of reasoning. The use of linguistic variables and fuzzy if-then rules greatly facilitates the process of decision making.

Introduced in 1965 by Pr. Zadeh, fuzzy logic provides a qualitative way to describe system behavior and performance using linguistic rather than numerical variables [16]. The use of fuzzy logic greatly improves the interpretability of results and facilitates the decision-making process [17]. Existing applications of fuzzy logic in FC domain includes system control [18], energy management of hybrid sources [19,20], modeling [10], etc. To construct a fuzzy logic system, a combination of membership functions, fuzzy rules and logical operators i.e., AND and OR are employed. Numerical data are converted into linguistic ones using membership functions. Then, these membership functions are combined, using rules, to obtain output values. Generally, there are two ways to develop fuzzy rules: expert knowledge and automatic learning from data [21,22]. The weaknesses of the first kind consist in the limitation of human knowledge in complex systems and its disability to discover underlying process phenomena. Inconvenience of the later is the large number of rules that may be induced for complex system with a large number of variables. The selection of the most influential variables is thus critical to achieve a better interpretability of the rules [21].

In this paper, FC diagnosis is treated as a pattern recognition problem. Diagnostic rules are designed by a combination of the incomplete human knowledge and automatic learning from experimental data. The proposed method has the capabilities of: (1) automatic feature selection, which plays the role of selecting the most valuable and discriminant features regarding the target faults; (2) automatic discovery of the underlying data structure, which is achieved by an unsupervised classification method (e.g. fuzzy clustering); (3) decision-making ability, which relies on the diagnostic rules designed by fuzzy logic.

The paper is organized as follows: Section 2 deals with the description of the experiment platform and the configuration of operating conditions. The principle of the double-fuzzy diagnostic methodology is introduced in Section 3. In the following section, experimental results and corresponding analysis are given. Finally, discussions and conclusions are provided.

2. Experiment description

2.1. PEMFC system

A 2 kW test bench was built in our laboratory which can configure different operating conditions of a PEMFC stack [23]. The system studied in this paper consists in a 20-cell stack with an active surface area of 100 cm^2. Graphite bipolar plates and a commercial membrane electrode assembly (MEA)-Gore Primea series 5510 are utilized to assemble the PEMFC stack. The characterization of the stack performance was done by EIS measurements which were performed through a homemade high-voltage impedance spectrometer with a high compliance voltage of ±700 V and maximal current of 450 A. Further details about the test bench are available in Ref. [23].

Considering the water management issue, at a certain current level (current density $J = 0.2A\ cm^{-2}$), the influence of five operating factors were investigated, including anodic relative humidity (h_a), cathodic relative humidity (h_c), hydrogen stoichiometry (s_c), air stoichiometry (s_a) and the stack temperature (T). A fractional experimental design has been employed [24] and the configuration of operating conditions is shown in Table 1. As can be observed in the table, at least two operating factors are changed simultaneously between two adjacent points. Among the sixteen operating conditions, point 6 is set as the reference point (healthy, corresponding to nominal operating conditions), with anodic and cathodic humidity of 35% and 75% respectively, hydrogen and air stoichiometry of 1.8 and 3 respectively, and stack temperature of 80 °C.

2.2. EIS technique and considered faults

This part deals with two points: a brief overview of EIS technique and related fault types in this study.

2.2.1. EIS technique

EIS technique is proved to be a suitable and powerful tool for PEMFC characterization and diagnosis [5,25]. It allows measuring the stack impedance by applying a small sinusoidal current (or potential) signal on the stack and measuring the corresponding stack voltage (or current) over a wide frequency range. Impedance is thus obtained by dividing the alternating components of the stack voltage and current. It can be represented either in the form of real and imaginary parts (Nyquist plot) or in the form of its magnitude and phase angle changing along with frequencies (Bode plots). Nyquist plot is the most utilized representation form, while Bode plots provide additional useful information (explicitly the frequency) which cannot be readily obtained from the Nyquist plot [25].

As a non-destructive diagnostic tool, EIS applies a small AC signal to the constant stack current or voltage without perturbing the system from equilibrium [26]. It provides rich information about the processes and mechanisms occurring within the FC. Its capability of differentiating influences of various processes, such as charge transfer and mass transport processes, offers a better understanding of the physical phenomena occurring inside the FC. Electrochemical parameters such as internal resistance (the high frequency intercept of the impedance arc on real axis) and polarization resistance (the low frequency intercept) can be directly extracted from EIS and further utilized as health indicators. All these characteristics make it promising in FC diagnosis domain.

Typical applications of EIS in FC domain includes the optimization of the membrane electrode assembly (MEA) structure or the optimization of the operating conditions, diagnosis purposes and aging [5,25,26], etc. It can also be noticed that EIS can be performed on FC stacks using the power converter, thus requiring no additional sensors [27].

Table 1
Configuration of 16 operating conditions (where point 6 is the reference point).

Point n°	h_a (%)	h_c (%)	s_a	s_c	T (°C)
1	35	35	1.8	2	80
2	35	35	1.8	3	60
3	35	35	3	2	60
4	35	35	3	3	80
5	35	75	1.8	2	60
6	35	75	1.8	3	80
7	35	75	3	2	80
8	35	75	3	3	60
9	75	35	1.8	2	60
10	75	35	1.8	3	80
11	75	35	3	2	80
12	75	35	3	3	60
13	75	75	1.8	2	80
14	75	75	1.8	3	60
15	75	75	3	2	60
16	75	75	3	3	80

2.2.2. Validity conditions

Before performing further analysis based on EIS measurement, its validity should be verified at first. According to the literature, four mathematical criteria, i.e., linearity, causality, stability and finiteness, must be met for a valid EIS measurement [28]. Herein, linearity and stability are highlighted considering their importance for EIS implementation.

(1) Linearity. To respect the linearity condition, the FC stack should work in a linear or quasi-linear region. In regard of this, the polarization curve was measured before the implementation of EIS in order to determine the linear operating region of the stack. In terms of the impedance, the acquired impedance should be irrelevant to the amplitude of the AC perturbation signal. Nevertheless, certain constraints should be met [29,30]. Firstly, the amplitude of the AC signal should be larger than the system intrinsic noises to guarantee a good signal-to-noise ratio. Secondly, the amplitude should not be so large to disturb the system from equilibrium. Numerous research has been carried out to investigate the influence of AC signal's amplitude on the impedance measurement [29,31]. A suggested range for its amplitude in Galvanostatic mode is 5%–10% of the stack DC current.

(2) Stability. The stability condition requires that the system works in the same stable state before and after each EIS measurement. To respect this condition, the FC stack should be brought to a stable operating state before starting each measurement. Normally, at least 30 min are needed to achieve a stable operating state. The EIS measurements should also be stationary, which means it is time-independent [28]. This condition can be easily verified by repeating the measurements and checking the consistency of the Nyquist plot or Bode plots. In regard of this, each impedance measurement under each operating condition in our study was repeated three times. As illustrated in Fig. 1, good consistencies can be observed on the EIS measurements obtained under both normal operating condition (pt6) and an abnormal operating condition (pt1).

2.2.3. Considered fault types

Concerning the water management issue, FC design and the choice of materials play a crucial role [32,33]. However, these factors are not in the scope of this study. Considering a given FC stack,

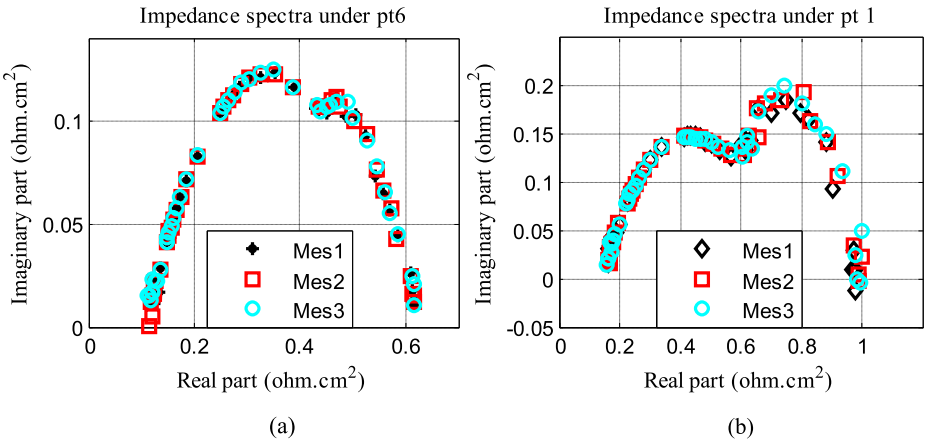

Fig. 1. Three EIS measurements under (a) normal operating condition pt6 and (b) abnormal operating condition pt1, where "Mes *n*" represents the *n*th repetition.

operating conditions are an important factor which influences greatly the water behavior inside the stack. In this paper, five parameters: anodic/cathodic relative humidity, stack temperature and air/hydrogen stoichiometry rates are configured with the purpose of introducing flooding and drying out operating conditions into the stack.

The influence of each parameter and their combination effects have been much studied in the literature [6,33,34]. Table 2 summarizes briefly five possible causes of drying out and flooding. Corresponding reflections on the EIS spectrum are also demonstrated. It should be underlined that the influence of each operating parameter is often interacting and also depends on the configuration of the other operating parameters.

In this study, the considered faults involve different degrees of flooding and drying, including severe, medium and slight ones. In order to test the validity of the developed algorithm, experimental data acquired at a low current density of 0.2A cm^{-2} are utilized in Section 4 and drying phenomenon is emphasized on.

3. Fuzzy-rule based classification methodology

3.1. The proposed diagnostic methodology

Fig. 2 illustrates the main idea of the developed methodology (an example of two-dimensional feature space is applied). A fuzzy clustering algorithm is applied to classify inputs and explore the underlying data structure, while fuzzy logic is further utilized to develop the diagnostic rules based on the labeled data. This also explains the meaning of "double-fuzzy". The proposed diagnostic methodology initially extracts and selects the most valuable features from EIS measurements. Feature space is further constructed where fuzzy clustering is performed to obtain different clusters. In the next step, fuzzy rules are then designed based on the clustering results with each rule corresponding to one cluster.

Three aspects are concerned herein: (1) how to extract and select features; (2) which kind of fuzzy clustering algorithm should be utilized; (3) how to design diagnostic rules based on the labeled clusters. In the following subsections, the above aspects are stressed on.

Table 2
Influences of the operating parameters.

Possible causes	Drying out case	Flooding case	Possible effects on EIS spectrum	Drying out case	Flooding case
Current density	↓	↑	Charge/mass transfer loop	↑	↓
			Internal resistance	↑	↓
Stack temperature	↑	↓	Mass transfer loop	↓	↑
			Internal resistance	↑	↓
Relative humidity	↓	↑	Charge transfer loop	↓	↑
			Internal resistance	↑	↓
Anodic stoichiometry	↑	↓	Charge transfer loop	↓	↑
			Internal resistance	↑	↓
Cathodic stoichiometry	↑	↓	Charge/mass transfer loop	↓	↑
			Internal resistance	↑	↓

3.2. Feature extraction and selection

Feature extraction and selection are performed in this section with the objectives of: (1) representing the original data with a much lower dimensionality; (2) selecting the most relevant and informative features to improve the interpretability of the results; (3) reducing the time and space complexity of the developed algorithm.

3.2.1. Feature extraction

Based on EIS measurements, feature extraction can be performed by building an equivalent circuit model with its critical parameters as useful features [35], or by establishing a mathematical model which approximates the spectrum [12], or directly based on expertise knowledge. Considering online implementation, the last method is adopted regarding its less computational effort and high efficiency.

A typical spectrum consisting of a charge transfer process (high frequency loop) and a mass transport process (low frequency loop) is shown in Fig. 3.

According to the literature, relevant features in the spectrum characterizing health status of the FC stack include: (1) Internal resistance (R_{in}), which indicates the total Ohmic resistances of the FC stack, especially the membrane resistance [32,33] and reflects the membrane humidification level; (2) Polarization resistance (R_{polar}), which is a reflection of the global performance of the FC stack [12,26]; (3) Difference of the polarization and internal resistance (R_{dif}), which corresponds to the width of the spectrum in the real axis and is believed to be subjected to the degradation resulting from a loss in the mass transport rate of reactants [36]; (4) Maximal absolute phase value (*mp*) and (5) its occurring frequency (*mf*), with the former related to the degradation of the electrolyte membrane [36] and the occurring frequency proportional to the inverse of the time constant of the corresponding process [25]; (6) Maximal

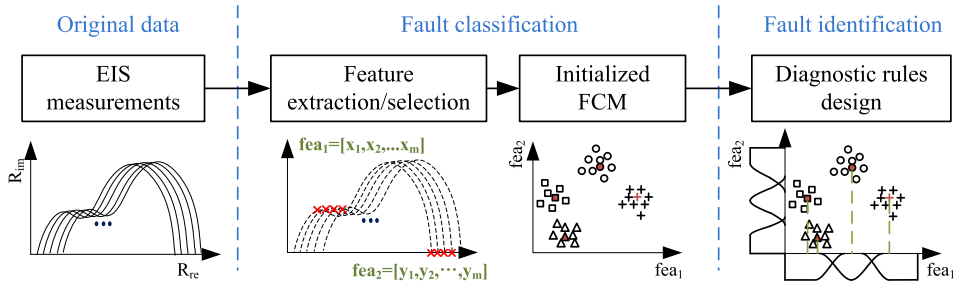

Fig. 2. Illustration of the double-fuzzy diagnostic methodology.

magnitude (*mm*), which is also included considering the case of incomplete spectrum where polarization resistance is not given or is difficult to measure [37].

3.2.2. Feature selection

Features selected according to expertise knowledge may contain high irrelevant and redundant information. More specifically, certain features may be irrelevant or less irrelevant to the target faults comparing with others; also there may be a high amount of redundant information contained inside the features which reduces the algorithm efficiency.

A main consideration about feature selection is to reserve the physical meaning of each feature in order to guarantee the interpretability. Hence, some well-known dimension-reduction methods such as principle component analysis (PCA), fisher discriminant analysis (FDA), and independent component analysis (ICA) are not applied here [38]. An automatic feature-selection method based on a two-step analysis, i.e., variance and correlative coefficient (CC) analysis is therefore developed [39]. Through this step, the dimension of the feature space can be determined with a good balance between the informative feature number and the computing effort for real-time implementation.

3.3. FCM initialized by subtractive algorithm

To design fuzzy rules by automatic learning from data, a fast, efficient and accurate partitioning algorithm is essential. Clustering algorithms provide interesting solution as they can easily discover the underlying phenomena of the data in the form of clusters. A widely used Fuzzy c-means (FCM) algorithm is considered here and further improvements are made based on it.

According to the literature, the performance of the traditional FCM can be greatly influenced by two factors: initial cluster centers or the initial membership values and the number of clusters. Typically, the initialization of the centers is set randomly which may increase the times of iterations and convergence. In addition, as FCM depends strongly on initial conditions, the algorithm is easy to trap into local optima and may lead to wrong and unstable classification results [40,41]. As for the number of clusters, it can be either given by the user according to expertise knowledge or be calculated by validity criteria, like partition coefficient (*PC*), Xie and Beni (*XB*) (more details in Subsecection 3.3.3), etc. In systems where expertise knowledge is incomplete, the determination of optimal number of clusters should be done automatically.

An initialized FCM method utilizing subtractive algorithm is developed here with the purposes of approximating the initial centers and determining automatically the number of clusters. The first subsection gives a brief introduction of the traditional FCM, while the second and the third subsections are devoted to the introduction of subtractive algorithm and validity indexes respectively. A diagram is depicted in Fig. 4 to illustrate the main idea of the initialized FCM algorithm.

3.3.1. Traditional FCM

Fuzzy c-means (FCM) clustering is one popular unsupervised algorithm which can be used to organize data into different groups based on similarities among the data points. The potential of revealing the underlying data structures makes it suitable for applications like pattern recognition, machine learning and image processing [42]. Compared with hard clustering methods, FCM allows the data points to belong to several clusters simultaneously with membership degrees between 0 and 1, which is more natural. More details about the traditional FCM are referred to [43].

3.3.2. Subtractive algorithm

Proposed by Chiu 1994 [44], subtractive algorithm provides an efficient solution to locate initial cluster centers that approximate the actual ones. In the first step, each data point is considered as a potential center with a potential measure given by:

$$P_i = \sum_{j=1}^{N} e^{\frac{\left\|-4x_i - x_j\right\|^2}{r_a^2}} \quad (1)$$

where P_i is the potential value, r_a is a radius defining a neighborhood and $\|\cdot\|$ denotes the standard Euclidean distance norm. The influence of a data point decays exponentially with the square of the distance. Obviously, the more neighboring data points inside

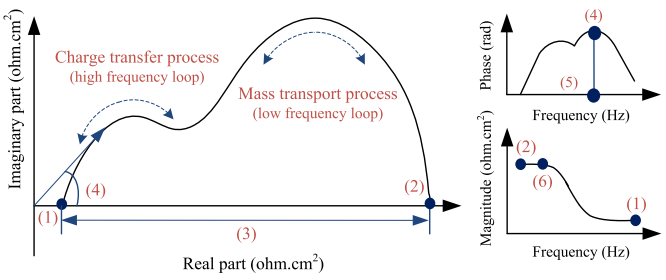

Fig. 3. Typical spectrum with two frequency loops.

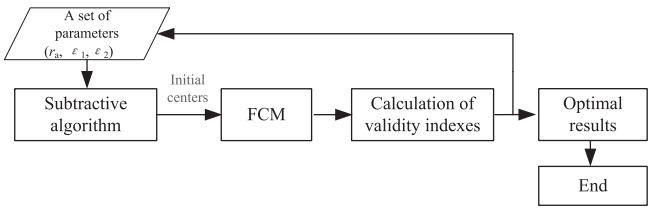

Fig. 4. Initialized FCM with subtractive algorithm.

the radius a data point has, the bigger potential value it will have. After each point's potential value is calculated, data point with the highest value will be chosen as the first cluster center.

In the second step, potential values of other data points are revised according to their distances to the first cluster center. Let x_1^* be the first chosen center and P_1^* be the corresponding potential value. The revised formula is defined as:

$$P_i \leftarrow P_i - P_1^* e^{\frac{-4\|x_i - x_1^*\|^2}{r_b^2}} \tag{2}$$

With r_b a penalty radius which avoids closely spaced cluster centers. If a data point is near the first cluster center, its potential value will be punished and its possibility to be chosen as the second center will be greatly reduced. A typical choice of r_b is $1.5r_a$. Among all the revised potential values the data point with the biggest potential value will be chosen as the second cluster center. The same process continues until the following criteria are satisfied:

if $P_k^* > \varepsilon_1 P_1^*$, the kth *center* is accepted;

if $P_k^* < \varepsilon_2 P_1^*$, the kth center is rejected.

where P_k^* represents the kth data point to be selected, ε_1 is the acceptance ratio and ε_2 is the rejection ratio. For determining the number of clusters, three parameters may have influences and need to be specified: r_a, ε_1 and ε_2. In light of this, validity indexes are introduced to provide some criteria for determining the optimal values of these parameters.

3.3.3. Validity indexes

Generally, two categories of validity indexes can be summarized: those considering only the compactness of each cluster and those taking into account both the compactness and separation of the clusters. Four validity indexes are considered in this subsection, including two indexes belonging to the first category, i.e., partition coefficient (V_{pc}) [34] and modified PC (V_{mpc}) [45], and two others related to the second one, i.e., Xie and Beni (*XB*) [46] and partition index (*SC*) [47]. For V_{pc} and V_{mpc}, a larger value of the measure indicates compacter clusters. Meanwhile, for *XB* and *SC*, an optimal clustering result is obtained when the smallest value is reached.

For the case of fault diagnosis, a good separation between-class and a high similarity within-class is highly desired. As mentioned above, the last two indexes (i.e., *XB* and *SC*) consider both the separation among the clusters and the compactness of each cluster. Their characteristics correspond well to the context of fault diagnosis, and they can be utilized as primary criteria. Meanwhile, the first two indexes focus on the compactness of each cluster. They can also be applied here to provide some supplementary references.

3.4. Mining interpretable diagnostic rules

As shown in Fig. 4, the last phase of the diagnostic methodology deals with mining interpretable fuzzy rules based on the clustering results. Generally, a fuzzy logic system consists in four fundamental components [48]:

(1) A rule base of fuzzy rules which describe relationship between inputs and outputs;
(2) A database defines membership functions for both inputs and outputs;
(3) A fuzzy inference system which performs inference procedure;
(4) The fuzzification and defuzzification processes.

As mentioned in Subsection 3.1, fuzzy rules will be designed by automatic learning from data. Through performing unsupervised clustering in the former subsection, underlying data structure is discovered and represented in the form of clusters. Each cluster is afterward labeled as a certain health status of the FC stack, according to operating condition and expertise knowledge. In the fuzzy logic system, each fuzzy rule is designed corresponding to a cluster. Thus the number of rules equals the number of clusters.

As for the membership function, a Gaussian function is used for the input variables supposing that data points inside each cluster satisfy statistic characteristic [15]. Multidimensional cluster centers $V = [v_1, v_2, \ldots, v_c]$ are projected along each dimension i ($i = 1, 2, \ldots, n$) of the feature space with the kth center fuzzified as:

$$A_k^{(i)}(x) = \exp\left[-\frac{\left(x - w_k^{(i)}\right)^2}{2\left(\delta_k^{(i)}\right)^2}\right], \quad k = 1, 2, \ldots, c \tag{3}$$

where w_k is the center of the k th membership function, δ_k is the corresponding variance, and c is the numbers of clusters. In order to determine the values of w_k and δ_k, a cut-point method in Ref. [15] is adopted here with cut points ($c + 1$ for each dimension) defined as:

$$t_k^{(i)} = \begin{cases} 2m_i - t_1^{(i)}, \text{for } k = 0 \\ \dfrac{v_k^{(i)} + v_{k+1}^{(i)}}{2}, \text{for } 0 < k < c \\ 2M_i - t_{c-1}^{(i)}, \text{for } k = c \end{cases} \tag{4}$$

where m_i and M_i are the minimum and maximum values of the ith dimension respectively, and $t_1^{(i)}, \ldots, t_k^{(i)}$ are the cut points of the ith dimension. w_k and δ_k are further calculated according to the following relationships:

$$w_k^{(i)} = \left(t_{k-1}^{(i)} + t_k^{(i)}\right)\Big/2 \tag{5}$$

$$\delta_k^{(i)} = \frac{t_k^{(i)} + t_{k-1}^{(i)}}{2\sqrt{-2\ln\varepsilon}} \tag{6}$$

where ε is the maximum overlap of two adjacent fuzzy sets (0.2 in our case).

As for the fuzzy inference system, there are generally two types: the Mamdani type and the Sugeno type [48]. The fundamental difference exists in the way of the outputs' generation, the former using a given defuzzification technique while the latter uses directly the weighted average of the output membership functions (chosen as being singletons) as the defuzzification technique. A zero-order Sugeno model is adopted herein considering its easiness and computational efficiency, with the form of:

If input 1 is A and input 2 is B, then output $= P$

where A and B are fuzzy sets, P is a crisp constant (also called singleton).

To summarize, mining diagnostic rules consists of three sequential steps: firstly, multidimensional cluster centers $V = [v_1, v_2, \ldots, v_c]$ are projected along each dimension i ($i = 1, 2, \ldots, n$) of the feature space. Gaussian membership function is applied to perform the fuzzification of the input variables of each dimension. Secondly, crisp outputs are defined by considering Sugeno inference system. Finally, fuzzy rules are designed which map the inputs to the outputs in combination with former clustering results.

4. Experimental description of the methodology and obtained results

4.1. Feature extraction and selection based on EIS measurements

4.1.1. EIS measurements

Eight representative stack spectra acquired at a low current density of 0.2 A cm^{-2} (I_{stk} = 20 A) are shown in Fig. 5 in the form of Nyquist plots. The frequency range of EIS goes from 5 kHz to 0.05 Hz with the amplitude of the AC signal equal to 7.5% of the stack DC current. The spectra plotted in the figures are normalized by dividing the number of cells (20) and then multiplied by the active surface area (100 cm^2).

A low current density is prone to the occurrence of drying out due to the insufficient water generated by the oxygen reduction reaction (ORR) process. In this circumstance, operating conditions play a crucial role on the hydration state of the FC stack in order to produce different degrees of drying out.

From an initial observation of Fig. 5, there is an obvious difference on the sizes of the two frequency loops under sixteen operating conditions. In some spectra, the low frequency loop prevails which corresponds to a more difficult mass transport process, e.g. pt1, pt3 and pt9, while in some other spectra the high frequency loop related to the charge transfer process dominates, e.g. pt4, pt10 and pt12.

Furthermore, an obvious variation on the polarization resistances can be observed in Fig. 5, which reveals the distinct global performances of the FC stack. In the enlarged region, evident differences among the internal resistances can be conceived. This is one of the principle consequences of the drying-out phenomenon. Normally, a higher degree of drying out leads to a larger value of internal resistance. Another consequence of drying out is reflected on the augmentation of the high frequency loop (from 5 kHz to 10 Hz), which corresponds to the deceleration of the charge transfer process. Another consequence of the drying out is the augmentation of the low frequency loop (from 10 Hz to 0.05 Hz), which is caused by the decrease of oxygen reduction kinetics.

Additionally, certain spectra exhibit high irregularities (e.g. pt1 and 12), particularly at low frequencies (<1 Hz) and at high frequencies (between 5 kHz and 2 kHz). The artefacts at the high frequencies are possibly caused by the inductive disturbances of the dynamic load [31]. The low-frequency artefacts, however, are due to the system short-time instability caused by the current perturbation.

Bode plot provides additional information in frequency domain which cannot be easily read from Nyquist plot. Fig. 6 shows the corresponding Magnitude and Phase plots. An obvious discrimination of maximal magnitudes appears in Fig. 6(a), while the occurring frequencies of the maximal phase (*mf*) are mainly divided into two groups with one group between 20 and 40 Hz and the other between 100 and 300 Hz, as shown in the Phase plots of Fig. 6(b). Generally, *mf* is acquired at high frequencies (between 20 Hz and 300 Hz) in our spectra, meaning that it's a reflection of the rate of charge transfer process.

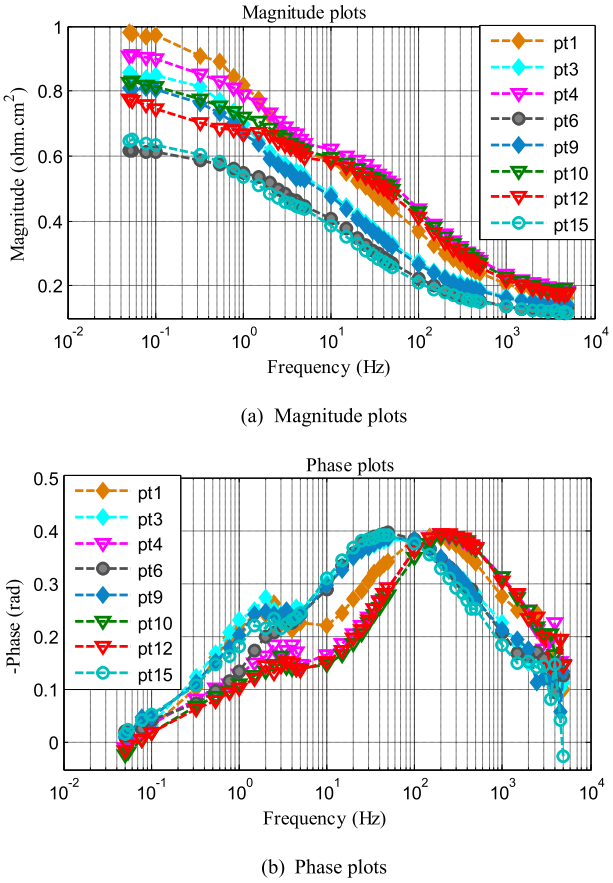

Fig. 6. Magnitude and phase plots under eight representative operating conditions.

4.1.2. Feature extraction and selection

In Subsection 3.2, according to the literature, six features related to the health status of the stack are listed and in this part they are extracted from the above spectra. Before the two-step analysis, all

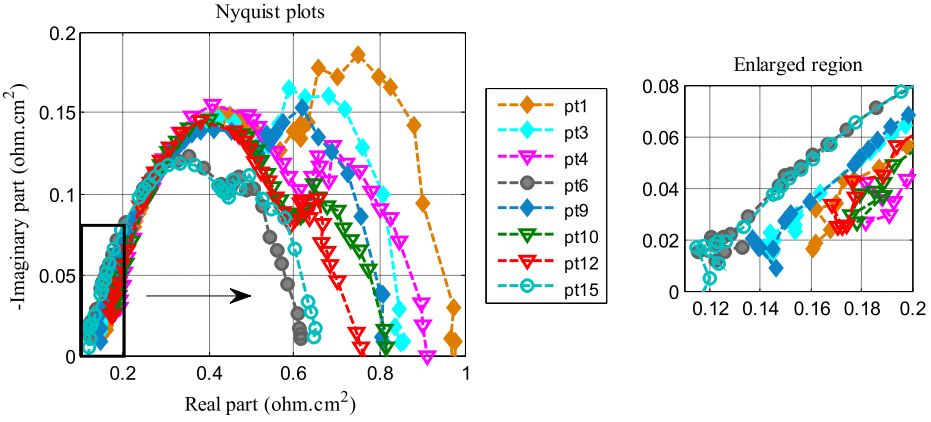

Fig. 5. Nyquist plots under eight representative operating conditions (e.g. pt1 indicates stack spectrum under operating condition 1).

Table 3
Variance value of each feature vector (arranged from largest to smallest).

mf	R_{in}	R_{polar}	*mm*	R_{dif}	*mp*
0.1297	0.1211	0.0941	0.0941	0.0862	0.0610

Table 4
Correlative coefficients among the features.

CCs	*mf*	R_{in}	R_{polar}	*mm*	R_{dif}
mf	1	0.9107	0.5475	0.5471	0.4208
R_{in}	0.9107	1	0.7965	0.7960	0.6945
R_{polar}	0.5475	0.7965	1	1.0000	0.9882
mm	0.5471	0.7960	1.000	1	0.9883
R_{dif}	0.4208	0.6945	0.9882	0.9883	1

the features are normalized into the range of [0, 1], considering their different units and variation ranges.

Table 3 shows variance analysis results of each feature. The feature with the maximum variance value is considered as the reference feature, i.e., *mf*. If the variance value is inferior to 50% of the maximum value, the corresponding feature is discarded, i.e., *mp* in our case. The consideration is that representative feature under different operating conditions should show sufficient variances; otherwise it could be considered as less relevant to the target faults.

Afterward, CCs among all the features are calculated as shown in Table 4 to reflect the redundancy contained in the features. As in the first step, *mf* is chosen as reference feature, its CCs with the others are calculated successively. One principle should be followed when performing CC analysis: If CC value among two features is higher than a threshold value (0.9 in our case), such as *mf* and R_{in}, feature with smaller variance value will be eliminated, i.e., R_{in} in the example. *mm* and R_{dif} are also eliminated as they have high relevancies with R_{polar}, 1.0 and 0.9882 respectively.

According to the automatic feature selection procedure, two features, i.e., *mf* and R_{polar}, are selected. It should be noted that R_{polar} and *mm* can be regarded as equivalent herein since their CC value equals 1.

4.2. Initialized FCM results

Based on the selected features, a feature space is constructed where FCM is performed to obtain the clusters. As indicated in Subsection 3.3, in order to initialize the FCM by subtractive algorithm, three parameters need to be determined: r_a, ε_1 and ε_2. The influence of each parameter (with the other parameters fixed) on the clustering performance is studied in this subsection, including r_a (0.1–0.9), ε_1 (0.4–0.9) and ε_2 (0.15–0.35). An example of studying the influence of r_a is shown in Table 5 and Fig.7, where Center_*n* is the corresponding number of clusters, V_{pc}, V_{mpc}, *XB* and *SC* are the four validity indexes.

As summarized in Subsection 3.3, *XB* and *SC* are taken as primary criteria, while V_{pc} and V_{mpc} provide supplementary information. It can be discovered that when $r_a = 0.4$, a local minimum value of *XB* is reached which indicates the clusters with both good compactness and separation. *SC* presents a monotonous increasing tendency. V_{pc} and V_{mpc} reach local maximum which represents relatively compact clusters. Therefore, $r_a = 0.4$ could be considered as an ideal choice. The corresponding number of clusters is 4.

The influences of ε_1 ($r_a = 0.4$, $\varepsilon_2 = 0.15$) and ε_2 ($r_a = 0.4$, $\varepsilon_1 = 0.5$) on the validity indexes *XB* and *SC* are presented in Fig. 8. It can be found that the algorithm performance is not so critical on the two parameters, since a wide range of the two parameters can give good clustering results.

Through a detailed study of the three parameters, the optimal clustering results can be obtained when: $r_a = 0.4$, $\varepsilon_1 = 0.4$–0.9, $\varepsilon_2 = 0.05$–0.15. In the following part, a combination of $r_a = 0.4$, $\varepsilon_1 = 0.5$ and $\varepsilon_2 = 0.15$ is applied to initialize the FCM algorithm and the clustering results are shown in Fig. 9.

As mentioned in Section 3.3, the performance of the traditional FCM can be greatly influenced by the random initialization. In order to see its performance dependence upon the initialization, the traditional FCM is executed 100 times successively. During the 100 executions, three types of clustering results are obtained, named type 1, 2 and 3, as plotted in Fig. 10. Among them, type 1 reaches the global minimum with an objective function value of 0.177, while the other types achieve local minima (0.261 and 0.262 respectively), as listed in Table 7. This implies that unstable and wrong clustering results may be obtained by the traditional FCM. Hence, it's quite necessary to perform the initialization of FCM and in such a way to ensure the robustness of the algorithm against this step.

As it can be observed in Fig. 9, initial centers located by subtractive algorithm are quite close to the actual ones, which greatly reduce the iteration steps in FCM. As shown in Table 6, clustering results and the computational time are recorded for both the traditional FCM and the initialized version during 100 executions. The percentage in the table represents the proportion of each type of clustering result (i.e., type 1, 2 and 3) obtained during the 100 executions. It can be observed that compared with the traditional FCM algorithm, the initialized version has more stable performance and always achieves the global minimum. Additionally, by comparing the average, maximum and minimum time consumed, it seems more computationally efficient.

Table 6
Performance comparison of the traditional FCM and initialized FCM.

	Type 1	Type 2	Type 3	aveTime (s)	maxTime (s)	minTime (s)
Initialized FCM	100%	0	0	0.0010	0.0018	0.0009
FCM	32%	36%	32%	0.0011	0.0022	0.0008
Obj. fun	0.177	0.261	0.262			

4.3. Mining interpretable diagnostic rules

Clustering results provide a knowledge base for diagnostic rules' design. As shown in Fig. 9, four clusters are grouped, with 2, 3, 9 and 11 in cluster *b*, 1 and 4 in cluster *c*, 10 and 12 in cluster *d* and the rest of operating conditions in cluster *a*. To design diagnostic rules, each cluster should be labeled in the first step. Both the clustering result and the incomplete human knowledge can provide useful information.

Table 5
Influence of r_a ($r_a = 0.1$–0.9, $\varepsilon_1 = 0.5$, $\varepsilon_2 = 0.15$).

r_a	0.1	0.2	0.3	0.4	0.5	0.6	0.7	0.8	0.9
Center_*n*	9	7	5	4	3	3	2	2	2
V_{pc}	0.9552	0.9636	0.8897	0.9216	0.9196	0.9196	0.9626	0.9676	0.9676
V_{mpc}	0.9495	0.9575	0.8621	0.8955	0.8794	0.8794	0.9252	0.9353	0.9353
XB	0.0755	0.0675	0.1356	0.0618	0.0959	0.0959	0.0640	0.0651	0.0651
SC	0.0012	0.0104	0.0261	0.0337	0.0502	0.0850	0.1442	0.1483	0.1483

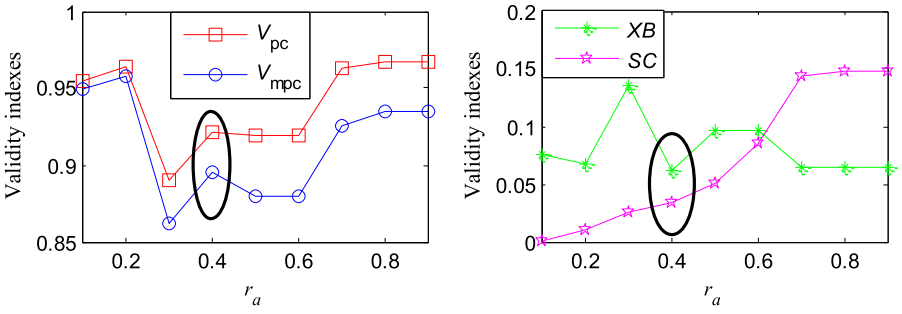

Fig.7. Influence of r_a on the validity indexes.

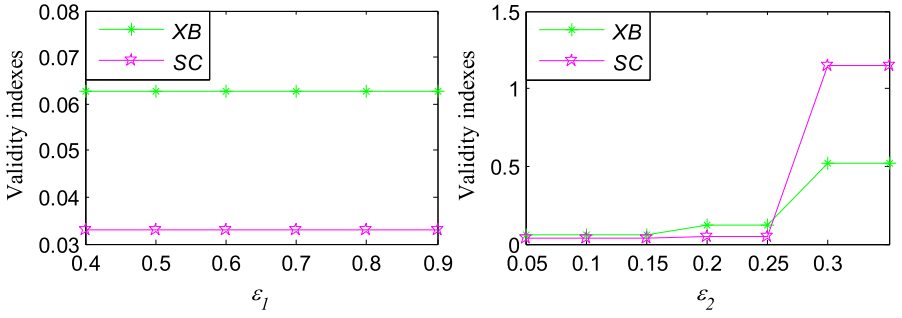

Fig. 8. Influence of ε_1 and ε_2 on the validity indexes *XB* and *SC*.

Part of the operating conditions is emphasized on in Table 7. In Section 2.2, the influence of each operating parameter is analyzed, including current density, stack temperature, anodic/cathodic relative humidity, and anodic/cathodic stoichiometry. According to the former analysis, it could be easily concluded that: 4 > 10; 12 > 9; 3 > 15, where ">" means drier. Combined with the clustering results, it can be further expressed as: *c* (1, 4) > *d* (10, 12) > *b* (9, 11, 2, 3) > *a* (15, 6, 5, 7, 8, 13, 14, 16).

Summarizing the above analysis, the four clusters obtained by initialized FCM algorithm are labeled as: *a*-healthy, *b*-slight drying, *c*-severe drying, *d*-medium drying. This also demonstrates the advantage of utilizing fuzzy logic in the case of incomplete human knowledge.

In the following step, a fuzzy logic system with two input variables (*mf* and R_{polar}) and one output SOH (state of health) is developed. Membership functions of the input variables are designed according to Equations (3)–(6). An example of input membership function of *mf* is shown in Fig. 11(a). For each input variable, three membership functions are designed, and their values are fuzzified as "small", "medium" and "big"/"large".

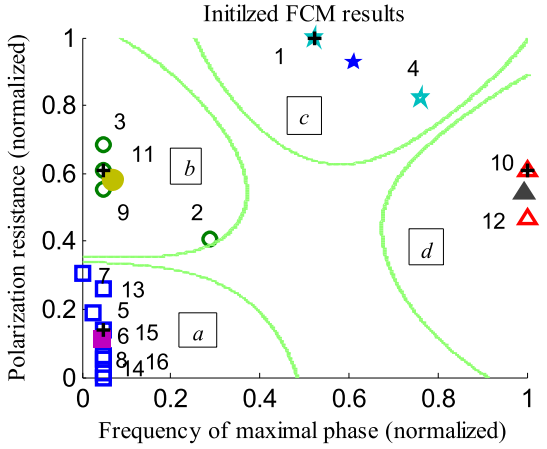

Fig. 9. Clustering results by initialized FCM ('+' indicates the initial cluster centers and filled makers are final located centers, letters in the rectangle represents the corresponding cluster).

A Sugeno type inference system is applied for the output design. Five singletons (0, 0.25, 0.5, 0.75,1) are designated for representing different health status of the stack, named "Out of range", "SevereDrying", "MediumDrying", "SlightDrying" and "Healthy", as illustrated in Fig. 11(b). A bigger value indicates a healthier status of the stack. For instance, "Healthy" corresponds to 1 while "SevereDrying" corresponds to 0.25.

Fuzzy rules which are designed according to the labeled clusters are underlined in Table 8, i.e., rules 1, 2, 6 and 8. For the region which is not covered by the clusters, "Out of range" is assigned as the consequent of the rule.

Based on the designed fuzzy rules, a diagnostic surface is obtained in Fig. 12, with yellow (in the web version) region corresponding to the healthy status (approaching 1), the light green region representing slight drying, the light blue region in the right side representing medium drying and the blue region in the left side on behalf of severe drying. The left regions of the surface are in deep blue and have a value approaching zero, which represents regions out of training range.

By performing the developed double fuzzy methodology, a set of fuzzy rules and corresponding diagnostic surface can be obtained with a high interpretability. They provide an important knowledge base for further online implementation. Additionally, they facilitate a good visualization of the stack health status. This is especially advantageous for online health monitoring of the FC stack.

4.4. Performance evaluation

In order to evaluate the performance of the developed methodology, 16 EIS measurements obtained under different operating conditions are used for off-line training, and another dataset of 16 measurements for online testing. A detailed procedure for online

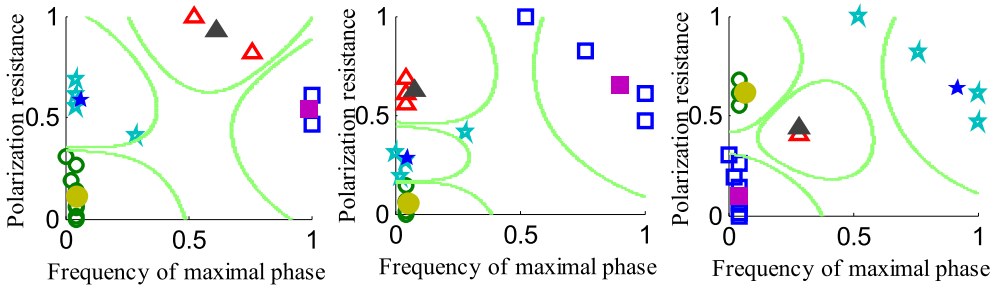

Fig. 10. Three different clustering results obtained by the traditional FCM (type 1, 2, 3, from left to right).

Table 7
Observation on the operating conditions (where pt6 is the reference point).

Point n°	h_a (%)	h_c (%)	s_a	s_c	T (°C)	Human knowledge
4	35	35	3	3	80	4 is drier than 10
10	75	35	1.8	3	80	
6	35	75	1.8	3	80	Normal condition
15	75	75	3	2	60	3 is drier than 15
3	35	35	3	2	60	
9	75	35	1.8	2	60	12 is drier than 9
12	75	35	3	3	60	

Table 8
Fuzzy-rule table.

1. If (*mf* is small) and (*mm* is small) then (SOH is "healthy")
2. If (*mf* is small) and (*mm* is medium) then (SOH is "SlightDrying")
3. If (*mf* is small) and (*mm* is large) then (SOH is "out of range")
4. If (*mf* is medium) and (*mm* is small) then (SOH is "out of range")
5. If (*mf* is medium) and (*mm* is medium) then (SOH is "out of range")
6. If (*mf* is medium) and (*mm* is large) then (SOH is "SevereDrying")
7. If (*mf* is big) and (*mm* is small) then (SOH is "out of range")
8. If (*mf* is big) and (*mm* is medium) then (SOH is "MediumDrying")
9. If (*mf* is big) and (*mm* is large) then (SOH is "Out of range")

testing is drawn in Fig. 13. It consists of two steps: feature extraction and fuzzy-rule table checking.

As for the 16-point test, a classification rate of 100% is achieved. Considering the online computational efficiency, the consumed time is proportional to the number of rules compared before fitting a rule ($O(n)$), which is quite computationally efficient.

Portability of the method is verified based on another dataset acquired from a different type of PEMFC stack called NEXA™ system. Air stoichiometry which may influence the oxygen availability as well as membrane humidity was configured with different values. More details about the stack and the configuration of operating conditions can be found in Ref. [37]. The same feature sets: the occurring frequency of maximal phase and maximal magnitude (equivalent to polarization resistance) are used for the construction of feature space. Finally, three kinds of health states, i.e., "high air flow", "normal" and "air starvation", are classified with success as demonstrated in Fig. 14(a). The corresponding diagnostic surface is plotted in Fig. 14(b).

5. Conclusions

In this study, the health state of a PEMFC stack was diagnosed based on a non-model diagnostic methodology in combination with the stack EIS spectra. The feasibility and interpretability of the methodology has been demonstrated. Several brief conclusions are made as follows:

(1) The proposed double-fuzzy diagnostic methodology consists of fuzzy clustering and fuzzy state-of-health determination, with the former to discover the underlying system phenomena and the latter to mine diagnostic rules. The whole procedure can be executed automatically.
(2) Two features, i.e., occurring frequency of the maximal absolute phase value and polarization resistance, are proved to

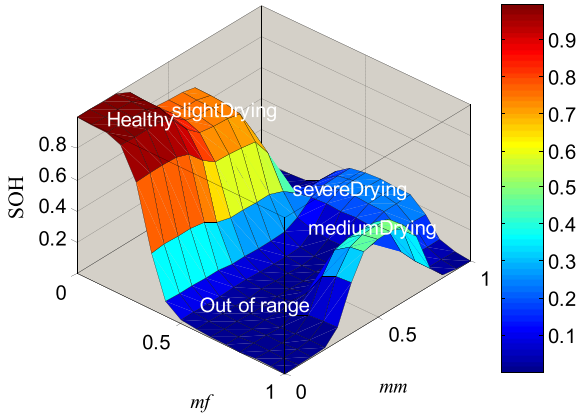

Fig. 12. Diagnostic surface based on the fuzzy rules.

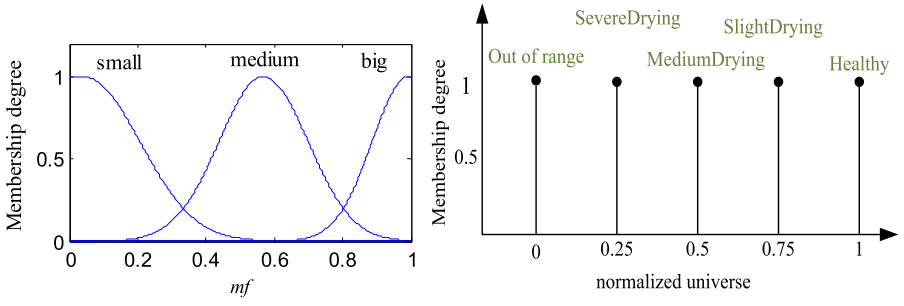

(a) Input membership function of variable *mf* (b) Output membership function

Fig. 11. Input and output membership functions.

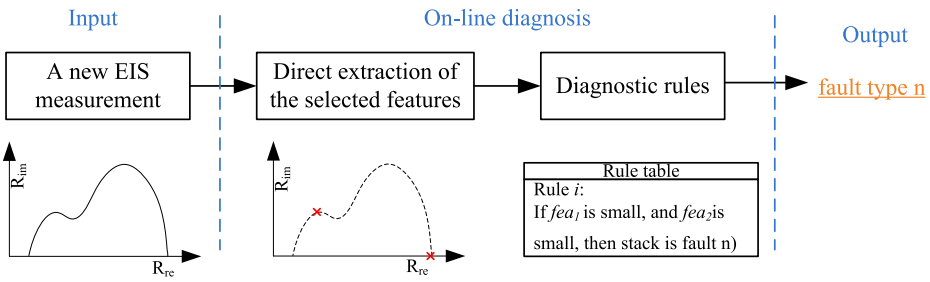

Fig. 13. Online testing procedure.

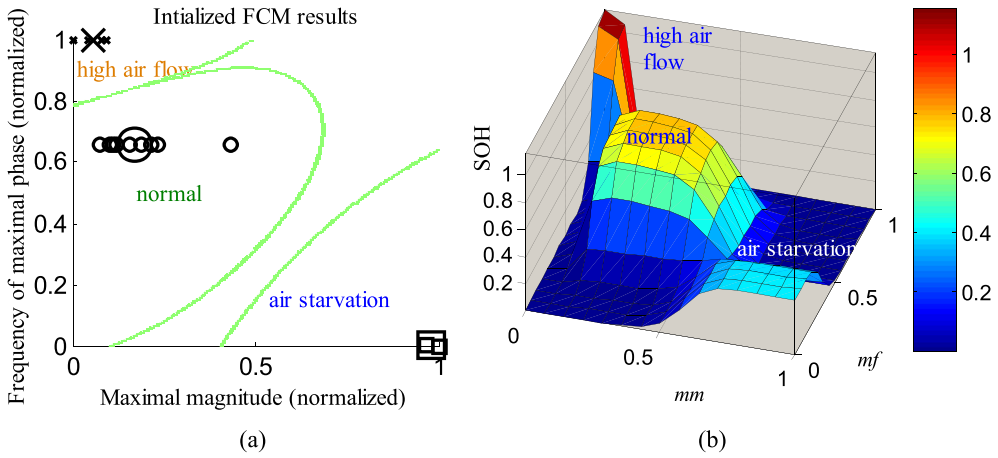

Fig. 14. Clustering results based on NEXA™ system (a) and the corresponding diagnostic surface (b).

be valuable and beneficial for further fault classification. They are extracted directly from EIS measurements and further selected via a two-step analysis called variance and correlative coefficient analysis. Feature extraction and selection are performed in such a way that the physical meaning of each feature is reserved in order to guarantee the interpretability of the later designed fuzzy rules.

(3) An initialized FCM algorithm utilizing subtractive algorithm is developed. More stable performance and higher computational efficiency are reached compared with traditionally used FCM. Furthermore, the optimal number of clusters can be set simultaneously.

(4) In order to perform fault identification, a two-input and one-output fuzzy logic system is designed based on the clustering results. Five health states of the stack are discriminated with easiness.

(5) Initial experimental results demonstrated the high accuracy rate of the developed methodology. Additionally, the methodology has high generalization ability as demonstrated by experimental results obtained from another type of PEMFC stack.

The developed diagnostic methodology is particularly advantageous in the following contexts: (1) Complex system with limited human knowledge; (2) A set of unlabeled data or unsupervised classification problem; (3) A requirement of high interpretability.

It should be noted that, since the diagnostic methodology is performed based on the stack impedance spectra, it hasn't the ability to locate the faulty cell in the stack. In the near future, the extensions will be made to cover the other kinds of faults as well, e.g. flooding. A more complete diagnostic rule base is expected to be established in order to be more powerful for online implementation. Additionally, based on the developed fuzzy rules and diagnostic surface, fuzzy control can be further added to take different measures according to the current health status of FC stack.

Acknowledgment

Experiment data from French ANR DIAPASON 1 project are greatly appreciated. The work performed was done within the European D-CODE project, funded under Grant Agreement 256673 of the Fuel Cells and Hydrogen Joint Technology Initiative. This project has been performed in cooperation with the Labex ACTION program (contract ANR-11-LABX-01-01).

References

[1] J.H. Wee, Renew. Sustain. Energy Rev. 11 (2007) 1720.
[2] M.-C. Pera, D. Candusso, D. Hissel, J.M. Kauffmann, IEEE Ind. Electron. Mag. 1 (2007) 28.
[3] Y. Wang, K.S. Chen, J. Mishler, S.C. Cho, X.C. Adroher, Appl. Energy 88 (2011) 981.
[4] 2012 Fuel Cell Technologies Market Report, U.S Department of Energy, 2013.
[5] X. Yuan, H. Wang, J. Colinsun, J. Zhang, Int. J. Hydrogen Energy 32 (2007) 4365.
[6] M. Ji, Z. Wei, Energies 2 (2009) 1057.
[7] R. Petrone, Z. Zheng, D. Hissel, M.C. Péra, C. Pianese, M. Sorrentino, M. Becherif, N. Yousfi-Steiner, Int. J. Hydrogen Energy 38 (2013) 7077.
[8] A. Hernandez, D. Hissel, R. Outbib, IEEE Trans. Energy Convers. 25 (2010) 148.
[9] Z. Li, D. Hissel, R. Outbib, S. Giurgea, Zürich, Switzerland, 2013.
[10] D. Hissel, M.C. Péra, J.M. Kauffmann, J. Power Sources 128 (2004) 239.
[11] N. Yousfi Steiner, D. Hissel, P. Moçotéguy, D. Candusso, Int. J. Hydrogen Energy 36 (2011) 3067.
[12] R. Onanena, L. Oukhellou, D. Candusso, F. Harel, D. Hissel, P. Aknin, Int. J. Hydrogen Energy 33 (2010) 2.
[13] J. Chen, B. Zhou, J. Power Sources 177 (2008) 83.
[14] N.Y. Steiner, D. Hissel, P. Moçotéguy, D. Candusso, Int. J. Hydrogen Energy 36 (2011) 740.

[15] G. Castellano, A.M. Fanelli, C. Mencar, in: J.V. de Oliveira, W. Pedrycz (Eds.), Adv. Fuzzy Clust. Its Appl., John Wiley & Sons, Ltd, 2007, pp. 211–228.
[16] S. Dash, R. Rengaswamy, V. Venkatasubramanian, Comput. Chem. Eng. 27 (2003) 347.
[17] J.A. Roubos, M. Setnes, J. Abonyi, Inf. Sci. 150 (2003) 77.
[18] A. Sakhare, A. Davari, A. Feliachi, J. Power Sources 135 (2004) 165.
[19] D. Gao, Z. Jin, Q. Lu, J. Power Sources 185 (2008) 311.
[20] O. Erdinc, B. Vural, M. Uzunoglu, J. Power Sources 194 (2009) 369.
[21] S. Guillaume, IEEE Trans. Fuzzy Syst. 9 (2001) 426.
[22] I. Gadaras, L. Mikhailov, Artif. Intell. Med. 47 (2009) 25.
[23] S. Wasterlain, D. Candusso, F. Harel, D. Hissel, X. François, J. Power Sources 196 (2011) 5325.
[24] B. Wahdame, D. Candusso, X. François, F. Harel, J.-M. Kauffmann, G. Coquery, Int. J. Hydrogen Energy 34 (2009) 967.
[25] S.M. Rezaei Niya, M. Hoorfar, J. Power Sources 240 (2013) 281.
[26] S. Asghari, A. Mokmeli, M. Samavati, Int. J. Hydrogen Energy 35 (2010) 9283.
[27] A. Narjiss, D. Depernet, D. Candusso, F. Gustin, D. Hissel, Electronics (2008) 734.
[28] A. Lasia, in: Mod. Asp. Electrochem., Springer, 2002, pp. 143–248.
[29] X. Yuan, J.C. Sun, H. Wang, J. Zhang, J. Power Sources 161 (2006) 929.
[30] R. Petrone, Electrochemical Impedance Spectroscopy for the On-board Diagnosis of PEMFC via On-line Identification of Equivalent Circuit Model Parameters, University of Salerno, 2014.
[31] S. Wasterlain, Approches Expérimentales et Analyse Probabliste Pour Le Diagnostic de Piles À Combistible de Type PEM, Université de Franche-Comté, 2010.
[32] H. Li, Y. Tang, Z. Wang, Z. Shi, S. Wu, D. Song, J. Zhang, K. Fatih, J. Zhang, H. Wang, Z. Liu, R. Abouatallah, A. Mazza, J. Power Sources 178 (2008) 103.
[33] N. Yousfi-Steiner, P. Moçotéguy, D. Candusso, D. Hissel, A. Hernandez, A. Aslanides, J. Power Sources 183 (2008) 260.
[34] S. Wasterlain, D. Candusso, D. Hissel, F. Harel, P. Bergman, P. Menard, M. Anwar, J. Power Sources 195 (2010) 984.
[35] N. Fouquet, C. Doulet, C. Nouillant, G. Dauphin-Tanguy, B. Ould-Bouamama, J. Power Sources 159 (2006) 905.
[36] D. Hissel, D. Candusso, F. Harel, IEEE Trans. Veh. Technol. 4 (2007) 1211.
[37] Z. Zheng, R. Petrone, M.C. Péra, D. Hissel, M. Becherif, in: IECON 2013, Vienna, Austria, 2013.
[38] Z. Zheng, R. Petrone, M.C. Péra, D. Hissel, M. Becherif, C. Pianese, N. Yousfi Steiner, M. Sorrentino, Int. J. Hydrogen Energy 38 (2013) 8914.
[39] Z. Zheng, M.C. Péra, D. Hissel, M. Becherif, Karlsruhe, Germany, 2013.
[40] X. Gao, Z. Xue, J. Li, W. Xie, in: 1998 Fourth Int. Conf. Signal Process. Proc. 1998 ICSP 98, vol. 2, 1998, pp. 1205–1208.
[41] Q. Yang, D. Zhang, F. Tian, in: 2010 Third Int. Conf. Intell. Netw. Intell. Syst., 2010, pp. 393–396.
[42] J.V. de Oliveira, W. Pedrycz (Eds.), Advances in Fuzzy Clustering and Its Applications, first ed., John Wiley & Sons, Ltd, 2007.
[43] J.C. Dunn, J. Cybern. 3 (1973) 32.
[44] S.L. Chiu, J. Intell. Fuzzy Syst. 2 (1994) 267.
[45] R.N. Dave, Pattern Recognit. Lett. 17 (1996) 613.
[46] X.L. Xie, G. Beni, IEEE Trans. Pattern Anal. Mach. Intell. 13 (1991) 841.
[47] A.M. Bensaid, L. Hall, J.C. Bezdek, L.P. Clarke, M.L. Silbiger, J.A. Arrington, R.F. Murtagh, IEEE Trans. Fuzzy Syst. 4 (1996).
[48] A.J. Salkind, C. Fennie, P. Singh, T. Atwater, D.E. Reisner, J. Power Sources 80 (1999) 293.